ARTICLE INFO
Article ID: 15-18-03-0016

doi:10.4271/15-18-03-0016

Deep Reinforcement Learning–Based Control Strategy for Electro-Hydrostatic Active Suspension

***Jiawei Wang,*[1,2,3] *Huiru Guo,*[1,2,3] *and Xiaohe Deng*[1,2,3]**

[1]*Wuhan University of Technology, China*
[2]*Wuhan University of Technology, Hubei Key Laboratory of Advanced Technology for Automotive Components, China*
[3]*Hubei Collaborative Innovation Center for Automotive Components Technology, China*

Abstract

A DRL (deep reinforcement learning) algorithm, DDPG (deep deterministic policy gradient), is proposed to address the problems of slow response speed and nonlinear feature of electro-hydrostatic actuator (EHA), a new type of actuation method for active suspension. The model-free RL (reinforcement learning) and the flexibility of optimizing general reward functions are combined with the ability of neural networks to deal with complex temporal problems through the introduction of a new framework called "actor-critic". A EHA active suspension model is developed and incorporated into a 7-degrees-of-freedom dynamics model of the vehicle, with a reward function consisting of the vehicle dynamics parameters and the EHA pump–valve control signals. The simulation results show that the strategy proposed in this article can be highly adapted to the nonlinear hydraulic system. Compared with iLQR (iterative linear quadratic regulator), DDPG controller exhibits better control performance, achieves the EHA control objective at faster speed, and notably improves the ride comfort and handling stability of the car. Moreover, DDPG's optimized valve–pump joint control strategy can reduce the energy consumption of the EHA system and improve the life of the hydraulic components while ensuring the control accuracy, solving the problem of low reliability of the active suspension system.

History

Received: 23 Jan 2025
Revised: 22 Apr 2025
Accepted: 20 Jun 2025
e-Available: 09 Jul 2025

Keywords

Electrostatic hydraulic actuator, Active suspension, Deep reinforcement learning

Citation

Wang, J., Guo, H., and Deng, X., "Deep Reinforcement Learning–Based Control Strategy for Electro-Hydrostatic Active Suspension," *SAE Int. J. Passeng. Veh. Syst.* 18(3):243–265, 2025, doi:10.4271/15-18-03-0016.

ISSN: 2770-3460
e-ISSN: 2770-3479

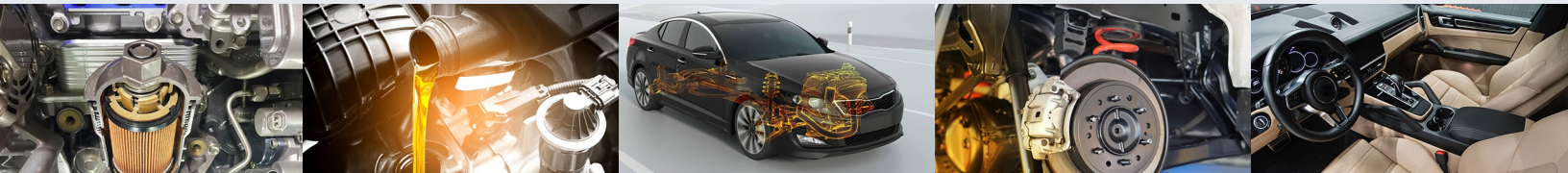

1. Introduction

The vehicle suspension system serves as the intermediary mechanism between the vehicle body and the road surface, playing a crucial role in supporting the vehicle body. A well-designed suspension system can significantly improve both ride comfort and driving stability. Suspension systems are primarily classified into three types: passive suspension, semi-active suspension, and active suspension. Among these, active suspension systems offer the greatest improvement in vehicle performance due to their ability to generate substantial active control forces. Based on the method of force generation, active suspension systems are further divided into hydraulic active suspension, pneumatic active suspension, and electromagnetic active suspension. Compared to passive and semi-active suspension systems, active suspension systems have more complex structures and require significant external energy input to generate control forces. Tseng and Hrovat [1] pointed out that active suspension control and semi-active suspension control are effective approaches to improve vehicle driving performance. While active suspension systems offer superior performance, they come with higher costs and complexity. The future development of active suspension will focus on more efficient actuators and advanced control algorithms.

Electro-hydrostatic actuators (EHA) are an important form of implementing this technology. However, since the response of EHA depends on the response of the motor and pump, it cannot meet the demands of high-load, high-response systems. Therefore, it is crucial to propose a control method that is highly compatible with EHA-based active suspension systems to meet the practical requirements of vehicle stability systems.

1.1. Related Work

The structure of the active suspension system is complex, which increases the difficulty of control. Two key factors influence the performance of the active suspension system: first, the accuracy of the active suspension system model, and second, the ability of the control strategy to adjust according to the actual driving scenarios of the vehicle.

Vehicle dynamics modeling is the primary step in active suspension design. When performing dynamic modeling, researchers typically have two options: the conventional approach simplifies the physical model, focusing on dividing the driving tasks into standard modules, breaking the vehicle model into several low-degree-of-freedom models, and connecting these independent modules using rule-based methods. This relatively simple, low-degree-of-freedom model is easier to control. However, since details are ignored during modeling, low-degree-of-freedom models deviate significantly from the real vehicle, leading to large errors during real-time control and resulting in potentially dangerous situations while driving. With the development of control theory, nonlinear control algorithms have emerged, adding complex dynamic behaviors to the vehicle model. The nonlinearities, uncertainties, and time delays in the actual operation of the active suspension system are considered, but this also presents significant challenges for controller performance. Therefore, the structural design and dynamic modeling of active suspension systems have gained increasing attention.

The electromagnetic active suspension uses linear motors or electromagnetic dampers to achieve active control. Yan and Yan [2] explained the working principle of the electromagnetic active suspension system, developed a mathematical model for it, and designed a complete system. The model was simulated and validated under random road inputs, proving the improved structural performance of the designed suspension. The electromagnetic active suspension offers advantages such as fast response speed, good controllability, and high mechanical efficiency. However, Turcotte et al. [3] found that the drawbacks of electromagnetic active suspension system are also significant. They conducted an in-depth experimental evaluation on the potential of MR (magnetorheological) actuators to improve vehicle ride comfort. Four high-power MR actuators were installed on a BMW 330Ci and tested on a closed test track. The results showed that the use of impedance controllers enhanced ride comfort. However, the MR actuators exhibited high energy consumption, required complex control algorithms due to their intricate structure, and had significantly higher manufacturing costs. Shafiekhani et al. [4] designed a robust controller using quantitative feedback theory (QFT) to address dynamic uncertainties in vehicle air suspension systems. The research focused on controlling linearized active air suspension systems. The nonlinearity and uncertainties of the pneumatic active suspension cannot be ignored, making it challenging to achieve precise displacement tracking or force-tracking control.

This article focuses on hydraulic active suspension. Compared to pneumatic active suspension, the hydraulic system offers better control accuracy and faster response speed. It also outperforms electromagnetic active suspension in terms of load capacity and cost. The key factors affecting the performance of hydraulic active suspension are actuators, control strategies, and energy consumption issues. Zhao and Yang [5] introduced a new hydraulic energy-regenerative vibration active suspension system. This system features continuous damping force adjustment from zero to maximum and high energy conversion efficiency, offering insights into addressing the energy consumption issues in hydraulic active suspension systems.

The actuator is a critical component of the hydraulic active suspension system. This article adopts EHA as the actuator for the active suspension. Traditional hydraulic active suspension systems regulate flow and pressure

using single valves or hydraulic pumps. Pressure adjustment is achieved through a central pump station, complex pipelines, and proportional valves. Luo and Gorges [6] proposed an adaptive robust force control method for pump-controlled EHA. This method can handle system parameter variations and external disturbances, ensuring precise control of the actuator output force. Compared to traditional hydraulic active suspension systems, EHA adopts a distributed electro-hydro-mechanical integrated design and a pump–valve coordinated control strategy, offering advantages such as compact structure, high power density, and fast response. For the EHA-based active suspension system, there are inevitable challenges such as increased control quantities, difficulty in system identification, and multi-agent synchronization, which require ensuring the robustness, accuracy, and multi-objective synchronization of the controller. Fully integrated, commercially available EHA active suspension systems are not accessible in the market right now. Several studies have already explored the deployment of EHA in active suspension systems and developed effective controllers to enhance suspension performance. Kou [7] used the bond graph model of EHA components to accurately establish a quarter-car dynamic model. Under specified road conditions and input parameters designed for the skyhook controller, experiments conducted with the EHA active suspension prototype and test bench demonstrated that the EHA active suspension significantly improves ride comfort, handling, and stability compared to passive suspension systems. Kou et al. [8] established mathematical models for a 2-degrees-of-freedom (2-DOF) active suspension and an EHA active suspension system. They analyzed the impact of the brushless DC motor on the system's dominant force. A force-tracking control strategy was designed, including an outer-loop LQG controller and an inner-loop motor speed and current controller.

The control methods mentioned above generally require precise mathematical models, and they are sensitive to system modeling errors. To address this issue, some studies have introduced DRL as a new design approach for intelligent agent behavior decision control. By utilizing the interactive training mechanism between the reinforcement learning agent and the environment, combined with deep learning for optimizing control decisions, the real-time decision-making performance has been enhanced, avoiding the complexity of traditional controller design. Miki et al. [9] proposed an intelligent motion control method for integrating proprioception and external sensory inputs using an attention-based recurrent encoder. The encoder is trained end-to-end to seamlessly combine different sensory modalities without relying on heuristic methods. The resulting motion controller exhibits high robustness and speed. Roy et al. [10] addressed the limitations of learning-based systems when deployed on robots, considering the agent as the key driver for the progress of machine learning technologies. The article emphasizes the unique challenges and opportunities of agents and suggests research directions to significantly advance the development of machine learning technologies. Since vehicle attitude control is a complex motion control problem, a machine learning–based end-to-end active suspension control method could be feasible. Machine learning, as a data-driven approach, allows algorithms to discover patterns from data, capture nonlinear relationships, and solve complex real-world nonlinear problems. Abadi et al. [11] introduced TensorFlow as an interface for expressing machine learning algorithms. Calculations expressed with TensorFlow can be executed across various heterogeneous systems with minimal modifications. The system is highly flexible and has been applied in 6the deployment of machine learning systems in production, covering over 10 fields including speech recognition, computer vision, robotics, information retrieval, and natural language processing. Hippalgaonkar et al. [12] identified transferable experiences from fields such as gaming, robotics, and materials research, including adaptive and accessible automation, employing hybrid (data-driven and model-based) algorithms to combine domain expertise and current learning in a cost-effective manner to solve high-complexity tasks. Ma et al. [13] explored a deep reinforcement learning (DRL) control method for position and attitude tracking of a biomimetic underwater vehicle (BUV). The algorithm uses the soft actor-critic (AC) algorithm SAC DRL method, training the controller through interaction with a simulated BUV. Chen et al. [14] summarized algorithms based on reinforcement learning and DRL for solving path planning problems in autonomous vehicles. DRL has been applied to vehicle vibration suppression, as it allows the design of reward functions based on multiple control objectives. Gheni et al. [15] established a quarter-vehicle model for a hub motor–driven electric vehicle, considering the vibrations of the seat, body, and unsprung mass, along with the time delays of the active and semi-active suspension. Using DRL algorithms, the model controls vertical vibrations via the active suspension. The model is trained for scenarios on random and speed bump surfaces. Moreover, the control performance is tested and compared with passive suspension and skyhook damping control strategies, followed by generalization tests of the deep reinforcement learning–based active suspension control strategy on random road surfaces.

This article proposes a new design approach for vehicle active suspension system control. By utilizing the reinforcement learning interactive AC training mechanism, combined with deep learning for optimal control decision-making, joint pump–valve control for the EHA-based active suspension system is achieved. Considering that hydraulic active suspension systems belong to high-dimensional continuous action spaces and have nonlinear characteristics, the DDPG algorithm is selected for controller training and deployment. The problems

addressed and the main contributions of this article are as follows:

1. In this article, EHA is used as an actuator for active suspension in automobiles. Unlike the traditional hydraulic active suspension, which adopts single hydraulic pump control or single servo valve control, the EHA system utilizes pump–valve joint control to improve the response speed and control accuracy, and the integrated structure also greatly reduces the size of the suspension system.
2. To address the nonlinear characteristics of EHA systems, this article proposes an active suspension control method utilizing DRL DDPG algorithm. The approach achieves end-to-end control between vehicle driving states and EHA hydraulic components. Through agent–environment interactive learning procedure, the method reduces dependency on precise system modeling while effectively adapting to and compensating for nonlinear behaviors in hydraulic active suspensions.
3. By constructing a real-time interactive training mechanism between the active suspension and the DDPG algorithm, the multi-objective control strategy of the active suspension is optimized by using the states of vehicle attitude angle and vertical acceleration as the feedback signals, so that the EHA active suspension system can realize accurate and fast response to road excitation under complex road conditions. The method innovatively solves the problem of the gap between the traditional model control and the actual system, and significantly improves the ride comfort and handling stability of the vehicle.

The rest of the article is structured as follows: Sections 2 and 3 introduce the EHA system model and the vehicle's 7-degrees-of-freedom model, respectively. Section 4 introduces the DDPG algorithm and applies it to decision-making and control of the EHA system. Section 5 presents simulation tests. Section 6 summarizes the article and outlines future research directions.

2. EHA Operating Principles and Modeling

2.1. EHA Operating Principles

The principle of pump–valve joint EHA system is shown in Figure 1. As can be seen from the figure, the pressure before the servo valve and the actuator force are determined by the permanent magnet synchronous motor and hydraulic pump. By controlling the motor speed, the hydraulic pump's output flow rate is adjusted, which in turn causes the pressure before the servo valve to reach the target value. The pressure difference and rod direction of the hydraulic cylinder are determined by the servo valve. By controlling the valve spool displacement, the servo valve's opening and the oil source ports are adjusted, which is reflected in the pressure difference between the high-pressure and low-pressure chambers of the double-acting hydraulic cylinder and the direction of the hydraulic cylinder's movement.

Compared to hydraulic active suspension with single pump drive, the acting direction of EHA hydraulic cylinder is determined by servo valve switching, which avoids the issue of high rotating inertia during motor commutation and improves the response speed. Additionally, instead of adjusting flow rate through a swash plate in a traditional variable pump, the flow is controlled by motor speed, reducing the complexity of the mechanism. This avoids the problem of the pump needing to rotate at high speeds when flow demand is low, reducing pump wear and power loss.

2.2. EHA System Architecture

The pump–valve coordinated EHA system uses a pump control subsystem combining a PMSM (permanent magnet synchronous motor) and a single-acting fixed-displacement vane pump. By adjusting the motor speed, this setup controls the pump's output flow. Its simple structure and compact size make it ideal for distributed

FIGURE 1 Schematic of pump–valve joint control EHA system.

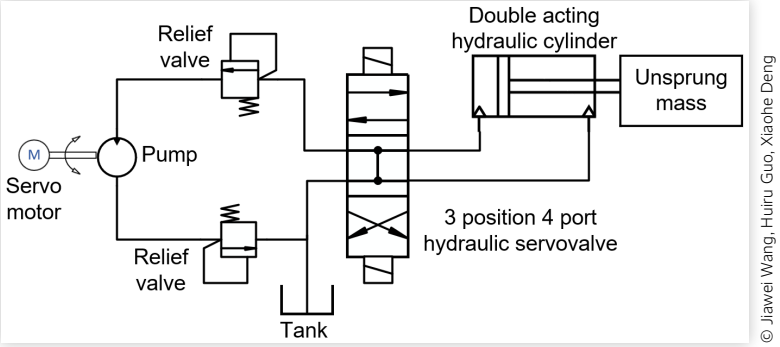

active suspension systems, offering high reliability, low cost, and easy industrial implementation.

To achieve high-precision control and fast dynamic response for the active suspension, a three-position four-way hydraulic servo valve works with the pump system for electro-hydraulic coordinated control. The actuator employs a double-acting single-rod hydraulic cylinder, enabling push–pull motion to handle road-induced reciprocating loads. The single-rod design saves space, while control strategies (e.g., adaptive algorithms) compensate for effective area differences across chambers, meeting varied load demands. This component selection optimizes energy efficiency, dynamic response, and structural compactness. The EHA system comprises four tightly integrated subsystems, each contributing to its superior performance in active suspension applications.

The mathematical model of a PMSM is as follows:

$$\begin{cases} u_d = R_s i_d + L_d \dfrac{di_q}{dt} - \omega_e L_q i_q \\ u_q = R_s i_q + L_q \dfrac{di_q}{dt} - \omega_e \left(L_d i_d + \psi_f \right) \end{cases} \tag{1}$$

where R_s is stator resistance; L_d and L_q are, respectively, rotor straight-axis inductor and rotor cross-axis inductor; ω_e is motor angular speed; ψ_f is permanent magnet chain.

The electromagnetic torque of the motor can be formulated as

$$T_e = \frac{3}{2} P_n \left[\psi_f i_q + \left(L_d - L_q \right) i_d i_q \right] \tag{2}$$

When the control strategy with $i_d = 0$ is selected for the motor, the expression for the electromagnetic torque can be simplified as

$$T_e = \frac{3}{2} P_n \psi_f i_q \tag{3}$$

When the motor mechanical loss torque and other loss torques are neglected, the mechanical equation of the motor can be simplified as

$$T_e - T_L = J_{pm} \frac{d\omega_r}{dt} + B_m \omega_r \tag{4}$$

where J_{pm} is the rotational inertia of the motor and the vane pump; B_m is the viscous damping coefficient of the motor; T_L is the load torque of motor, which can be formulated as:

$$\begin{aligned} T_L &= \left(K_{visc} + K_{fric} \right) \omega_m + D_p \left(P_a - P_b \right) \\ D_p &= \frac{D}{2\pi} \end{aligned} \tag{5}$$

where K_{fric} is the frictional resistance coefficient of the vane pump; K_{visc} is the viscous resistance coefficient of the vane pump; P_a and P_b are, respectively, the inlet and outlet pressures of the vane pump; D is the displacement of the vane pump.

Since the motor is directly connected to the vane pump, the torque acting on the vane pump is:

$$T_t = J_{pm} \frac{d\omega_m}{dt} + \left(K_{visc} + K_{fric} \right) \omega_m + D_p \left(P_a - P_b \right) \tag{6}$$

The vane pump output flow equation is:

$$Q_b = D_p \omega_m - L_{pi} \left(P_a - P_b \right) - L_{po} \left(P_b - P_T \right) - \frac{V_0}{\beta_e} \frac{dP_b}{dt} \tag{7}$$

In the formula, L_{pi} and L_{po} are, respectively, the vane pump internal and external dynamic leakage coefficient; P_T is the vane pump unloading port pressure; V_0 is the average volume of the pipeline and servo valve; β_e is the hydraulic oil volume modulus of elasticity

The flow–pressure relationship of the servo valve is formulated as:

$$P_L = P_s - \frac{\rho}{2} \left(\frac{Q_L}{C_d k_x x_v} \right)^2 \tag{8}$$

where C_d is the flow coefficient; k_x is the valve opening coefficient; x_v is the displacement of servo valve spool; P_s is the supply pressure; $P_L = P_1 - P_2$ is the load pressure.

According to the principle of flow continuity, the required flow rate in the high-pressure chamber of the hydraulic cylinder is.

$$Q_1 = A_p \frac{dx_p}{dt} + C_{po} P_1 + C_{pi} P_L + \frac{V_1}{\beta_e} \frac{dP_1}{dt} \tag{9}$$

where A_p is the hydraulic cylinder piston area; x_p is the hydraulic cylinder piston displacement; C_{po} and C_{pi} are the hydraulic cylinder external and internal dynamic leakage coefficients; V_1 is the hydraulic cylinder high-pressure chamber volume.

The force balance equation for a hydraulic cylinder is:

$$m_p \frac{dx_p{}^2}{d^2 t} + B \frac{dx_p}{dt} + K x_p = P_L A_p - F_l \tag{10}$$

where m_p is the mass of the piston; B is the viscous damping coefficient of hydraulic cylinder; K is the elasticity coefficient of the hydraulic cylinder; F_l is the load change on the piston rod.

Based on the EHA model, its nonlinear characteristics primarily arise from the following aspects. First, the inherent nonlinearities of the hydraulic system are significant. For example, the servo valve flow equation is

influenced by the square-root effect of the pressure difference across the valve port, resulting in a nonlinear relationship between flow rate and electrical signals. Second, the nonlinear coupling between the electromagnetic torque and current/speed in the PMSM, along with dynamic distortion caused by friction torque and leakage effects in the vane pump, further increases the complexity of system modeling. Additionally, Coulomb friction in the hydraulic cylinder, oil compressibility, and parametric uncertainties due to sudden load changes can significantly affect system stability and tracking accuracy.

3. Vehicle Dynamics Modeling

In this article, the ride comfort and driving stability of the car are analyzed, so the 7-degrees-of-freedom dynamics model of the car is established, and the 7-degrees-of-freedom model of the whole car (shown in Figure 2) can also be regarded as the vehicle driving model, which consists of the sprung and unspring masses, and the body is connected to four wheels through the springs, dampers, and hydraulic actuators at the four endpoints. The body has 3 degrees of freedom, including vertical motion, rolling motion, and pitching motion. The remaining 4 degrees of freedom are the vertical motion of each of the four wheels.

The 7-degrees-of-freedom vehicle dynamics model is employed to evaluate suspension performance, comprising:

Vertical Motions: Body vertical acceleration, pitch, and roll.

Wheel Dynamics: Vertical displacements of four wheels.

Suspension Interactions: EHA-generated forces at each wheel station.

This model captures critical coupling effects between suspension actuation and vehicle attitude while balancing computational efficiency for control design. The dynamic equations integrate EHA force outputs with inertial and road excitation inputs, enabling analysis of both ride comfort (body acceleration) and handling stability (pitch/roll angles). The full set of governing equations is presented in Appendix.

FIGURE 2 7-degrees-of-freedom model of the whole vehicle.

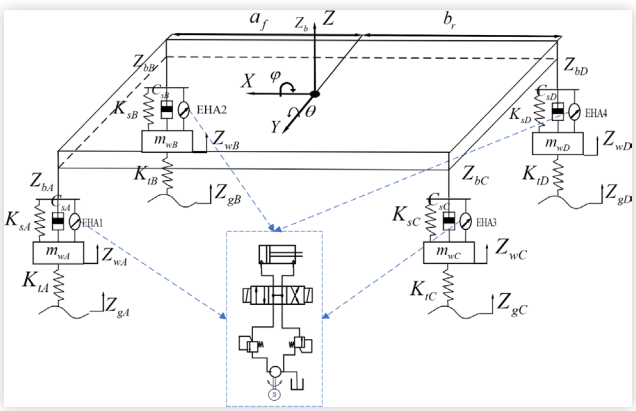

4. Deep Reinforcement Learning–Based Control Strategy

DRL is an important development in reinforcement learning and refers to reinforcement learning methods that use deep neural networks as models. The method uses neural networks to represent state value functions and policies to deal with high-dimensional state and action spaces, thus enabling the solution of problems that cannot be solved by traditional reinforcement learning algorithms.

Among many DRL algorithms, a DDPG algorithm, which is designed for a continuous action space, shows significant advantages in controlling complex dynamic tasks [16]. The DDPG algorithm uses the AC algorithm as its basic framework and utilizes a deep neural network to approximate the Q-value function, so that the policy network makes optimal actions and the evaluation accuracy of the value network is continuously improved. A neural network is used to approximate the Q-value function, while the stochastic gradient method trains both the policy network and the value network. This enables the policy network to make the optimal action a, and the accuracy of the value network's evaluation of q improve continuously. The introduction of the noise mechanism and the target network ensures the ability of exploring and the stability of the training, and many special advantages make the DDPG algorithm suitable for dealing with the control tasks in high-dimensional continuous action space.

4.1. AC Network

The AC method is a temporal difference method (TD method) that combines a value function–based method and a policy function–based method. Its framework is shown in Figure 3:

Where the policy function is the actor, which gives the action, and the value function is the critic, which evaluates the goodness of the action given by the actor and generates a TD signal to guide the updating of the value function and the policy function. As shown in Figure 3, after the actor of the policy network selects an action, the state of the environment is changed accordingly, and the critic evaluates the new state to determine whether

FIGURE 3 Schematic of actor-critic network.

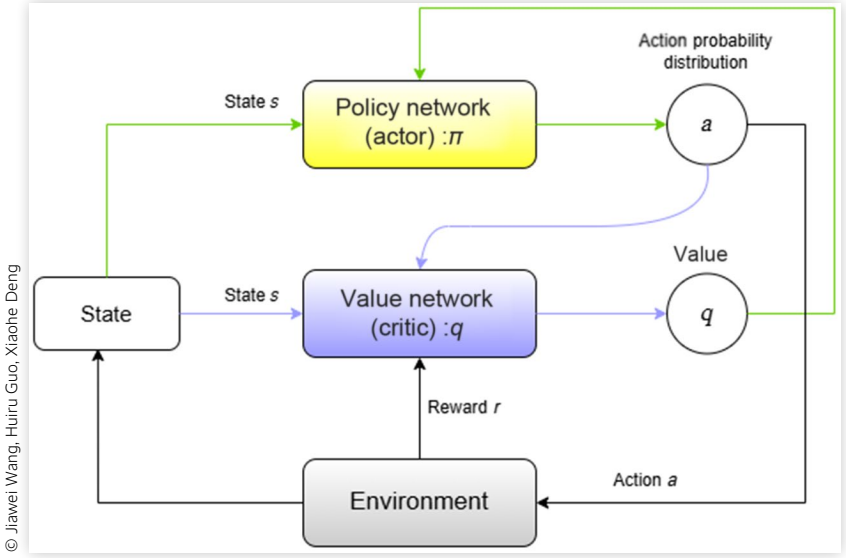

the action is good or bad, and the evaluation is based on the form of the TD error, with the following formula:

$$\delta_t = R_{t+1} + \gamma V_t\left(s_{t+1}\right) - V\left(s_t\right) \tag{11}$$

where R_{t+1} is the instant reward at moment t; V_t is a function of the value of the evaluation network at moment t; γ is the discount factor. If the TD error value δ_t is positive, the future choice of a_t should be increased, and if the TD error value δ_t is negative, the future choice of a_t should be decreased.

In the policy network, the choice was made to use the softmax activation function to compute the action probabilities:

$$\pi_t\left(a|s\right) = P_t\left\{s_t = a|s_t = s\right\} = \frac{e^{H_t(s,a)}}{\sum_b e^{H_t(s,b)}} \tag{12}$$

where $H_t(s,a)$ denotes the propensity of the state s to choose each action a at moment t.

Therefore, the increase and decrease in the choice of action a_t at moment t can be realized by an increase or decrease in $H_t(s,a)$:

$$H_{t+1}\left(s_t,a_t\right) = H_t\left(s_t,a_t\right) + \beta\delta_t \tag{13}$$

where β is the training constant.

Overall, for the case of an infinite number of possible action sets, unlike methods that only learn action values, the AC approach learns an explicit stochastic policy that determines the optimal probability of each action without searching for an infinite set of actions, dramatically reducing the amount of computation and increasing the speed of convergence of the policy.

4.2. Policy Network and Value Network Updates

In the policy neural network, $\pi(a|s;\theta)$ is used to complete the prediction of $\pi(a|s)$ and make the corresponding action, so that the action can be continuously optimized, where θ is the trainable parameter of the neural network. In the value neural network, $q(s,a;w)$ is used to complete the prediction of $Q_\pi(s,a)$ and evaluate the good and bad actions, and the training makes the evaluation more accurate, where W is the trainable parameter of the value neural network.

During the training process of DDPG, the policy network $\pi(a|s;\theta)$ is constantly updated to improve the state value function $V(s;\theta,w)$. During the update process, the supervision of the agent's action arises entirely from the evaluation of the action by the value function, and the agent is able to continuously improve its performance and make better actions even under supervision. The value network $q(s,a;w)$ is also constantly updated to better estimate the regression value, and during the update process, the supervision of the evaluation arises entirely from the reward value, and the evaluator's judgment becomes more accurate.

4.3. DDPG Controller Implementation

As shown in Figure 5, DDPG is implemented as the EHA active suspension controller. The implementation of the DDPG algorithm involves the design of the reward function r and the selection of termination conditions, where the choice of the reward function r is closely related to the vehicle's state s. This article divides the content of the reward function into the control objective

FIGURE 4 Suspension tuning with DDPG control setting.

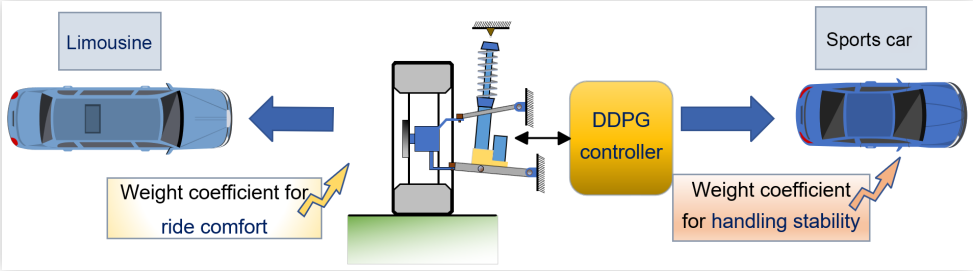

function and the implementation cost function. The control objective refers to the improvement of the vehicle's ride comfort and handling stability under DDPG control of the EHA active suspension. Key parameters include the vehicle's attitude angles, vertical acceleration, and the like. It is worth mentioning that the control objective function can be adjusted through the magnitude of the incentive coefficient. Specifically, the suspension system can actively select training weights for comfort and handling. If the vehicle has higher comfort requirements, the incentive coefficient for vertical acceleration can be increased. If the vehicle has higher handling stability requirements, the incentive coefficient for the vehicle's attitude angle can be increased. The control objective function gives the EHA active suspension system high-performance tuning flexibility, avoiding the complex performance adjustment process of passive or semi-active suspensions (Figure 4).

The implementation cost function consists of parameters from the EHA hydraulic system, specifically including the electric drive signal $\boldsymbol{u}$ of the hydraulic pump, the displacement $\boldsymbol{xv}$ of the servo valve, and the pipeline pressure $\boldsymbol{p}$. Active suspensions generally face issues of high energy consumption and low reliability. Therefore, optimizing the implementation cost function enables precise control of the hydraulic pump and servo valve in the EHA system. The pump's output flow can be adjusted based on the expected displacement of the hydraulic cylinder, avoiding hydraulic system overflow caused by continuous high-flow output. Precise control of the servo valve effectively reduces the switching frequency of valve positions, improving the response speed and lifespan of the valve (Figure 5).

In the whole vehicle model incorporating the electro-hydrostatic active suspension, the following observation vector, i.e., state s, is set up.

Pitch angle of the whole vehicle θ; pitch angle velocity ω_θ; roll angle φ; roll velocity ω_φ; vertical body displacement z_b; vertical velocity v_{zb}; vertical acceleration a_{zb}; hydraulic pumps-driven signals u_1, u_2, u_3, u_4; Servo valve displacement x_{v1}, x_{v2}, x_{v3}, x_{v4}; Actuating force of hydraulic cylinders F_1, F_2, F_3, F_4; Vertical displacement of the four end points of the body z_{b1}, z_{b2}, z_{b3}, z_{b4}; Four unsprung mass displacements of the body z_{w1}, z_{w2}, z_{w3}, z_{w4}; According to the above observation, the reward function $r_t = r_1 + r_2$ under each step length T_s is designed, which contains positive incentive r_1 and negative incentive r_2, and the positive incentive r_1 function at moment t is:

$$r_{1t} = \begin{cases} a_1\left(e_{1t-1} - e_{1t}\right) & e_{1t-1} > e_{1t} \\ 0 & e_{1t} \geq e_{1t-1} \\ a_2\left(e_{2t-1} - e_{2t}\right) & e_{2t-1} > e_{2t} \\ 0 & e_{2t} \geq e_{2t-1} \\ a_3\left(\ddot{Z}_{bt-1} - \ddot{Z}_{bt}\right) & \ddot{Z}_{bt-1} > \ddot{Z}_{bt} \\ 0 & \ddot{Z}_{bt} \geq \ddot{Z}_{bt-1} \end{cases} \tag{14}$$

where a_1 along with a_2 and a_3 are the excitation coefficient and the magnitude of the constant value can be adjusted according to the model-specific control strategy; e_1 is the difference between the vehicle vertical displacement and the initial value; e_2 is the difference between the vehicle attitude angle $[\theta, \varphi]$ and the initial value. If $e_{1t-1} > e_{1t}$ it means that the change in vertical displacement at the current step is smaller than the previous step, which can indicate that the action taken at the current step improves ride comfort, then the reward r_1 calculated from the difference between e_{1t-1} and e_{1t} at the moment t is considered as a positive incentive. Similarly, the improvement in attitude angle and body vertical acceleration will also be considered as positive incentive.

The negative excitation r_2 function is:

$$r_2 = -40e_1^2 - 2\dot{e}_1^2 - 10e_2^2 - 0.05\sum_i {x_{vt-1}^i}^2 - 2.5e^{-6}\sum_i {F_{t-1}^i}^2 - 0.5\ddot{z}_b^2 - 0.1\sum_i {u_{t-1}^i}^2 \tag{15}$$

After designing the reward function, termination conditions need to be set to prevent the agent from performing meaningless exploration that exceeds the

FIGURE 5 Operating principle of EHA active suspension under DDPG control.

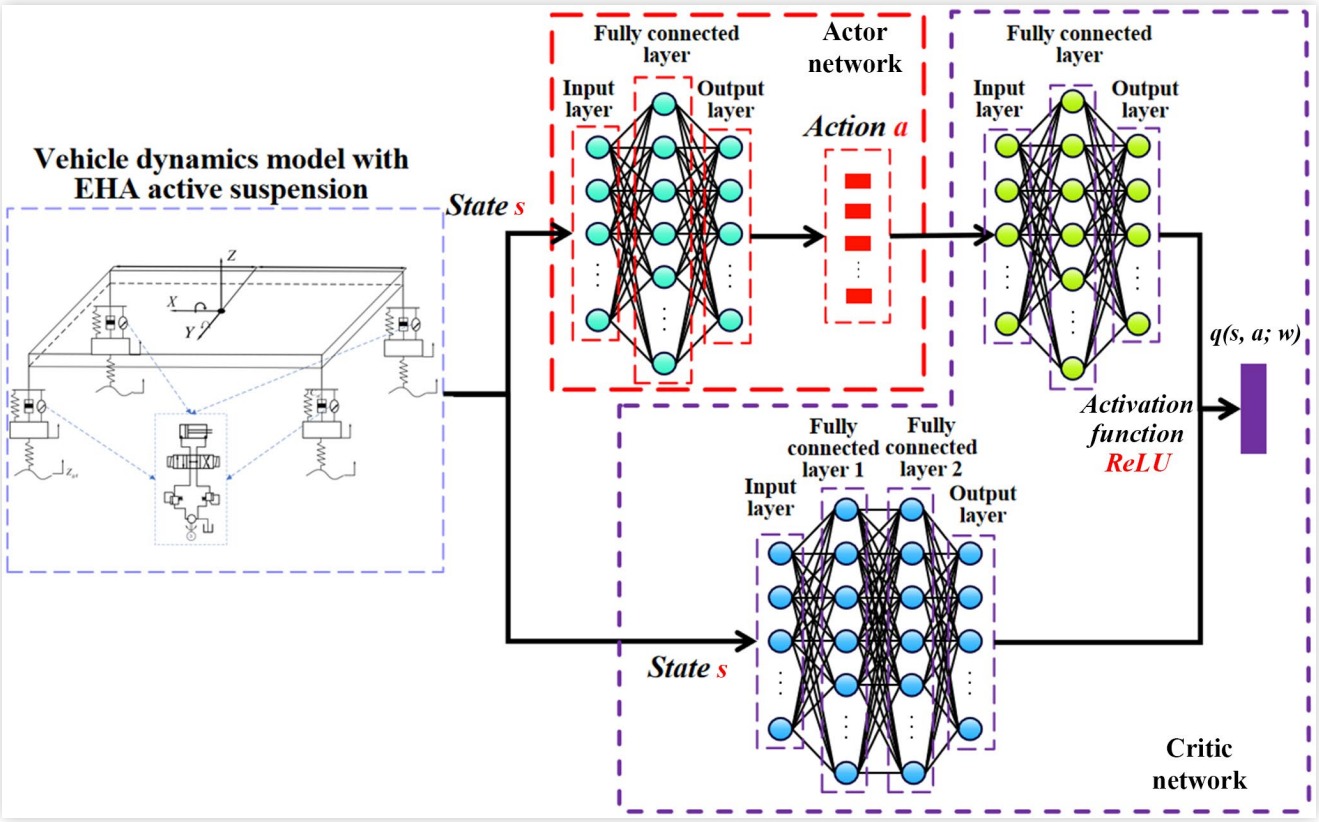

constraint conditions. When the agent meets the termination conditions, the current training process ends, and the next round of training begins with random parameters. Therefore, the setting of termination conditions has a significant impact on the training process. If the termination conditions are too lenient, the training time will increase, and the training results may not converge, leading to training failure. On the other hand, if the termination conditions are too strict, the agent's exploration ability will be limited, making it difficult to find an optimal solution that balances both local and global performance. In this article, the termination condition is set as follows: when the displacement of the four hydraulic actuators leads to the vehicle body's vertical displacement exceeding the threshold z_{bmax}, or the vehicle's roll angle and pitch angle exceed the threshold $[\theta_{max}, \varphi_{max}]$, the training will be terminated.

5. Simulation Test

The simulation tests in this article are run in MATLAB/Simulink software, and the DDPG-controlled EHA active suspension is verified to effectively improve the ride comfort and handling stability of the car by analyzing the parameters of the EHA active suspension with the application of the DDPG controller and the parameters of vehicle's 7-degrees-of-freedom dynamics model. In order to demonstrate the advantages of the DDPG algorithm in control performance, the dynamic performance of the suspension with DDPG control and variable-damping semi-active suspension along with iLQR control is compared and simulated.

5.1. Controller Simulation Training Analysis

The quality of the training process is primarily assessed based on the reward value and average reward value during the training. As mentioned earlier, the magnitude of the reward value is determined by the dynamic performance of the vehicle during operation. If the pump–valve joint EHA tracks the random road input well, effectively suppressing the vehicle's vertical acceleration, attitude angles, and other observed parameters, and the termination conditions have not been met, then the control system will receive a higher reward value. Conversely, if the tracking performance is poor or the termination conditions are met, the reward value will be lower. The hyper parameter of DDPG agent network is shown in Table 1.

TABLE 1 Hyper parameter of DDPG agent networks.

Hyper parameter	Value
Policy network learning rate	0.0001
Value network learning rate	0.001
Policy network fully connected layer	64
Value network fully connected layer1 (state path)	100
Value network fully connected layer2 (state path)	64
Value network fully connected layer2 (action path)	64

TABLE 3 EHA system parameters.

Parameter	Value
Fluid density (kg/m^3)	845
Quantitative pump displacement (ml/r)	30
Cross-sectional area of the piston (m^2)	7.5×10^{-3}
Cross-sectional area of the piston rod cylinder (m^2)	5×10^{-3}
Hydraulic cylinder piston stroke (m)	0.1
viscous damping coefficient of hydraulic cylinder [N/(m/s)]	1,000,000
Hydraulic oil volume modulus of elasticity (Pa)	1.5×10^9
elasticity coefficient of the hydraulic cylinder (N/m)	100,000

As shown in Figure 6, after approximately 2000 episodes of training, the agent's reward value starts to increase continuously, and the overall system performance improves accordingly. After 2300 episodes of training, the system's reward value begins to converge and fluctuates around 1500. At the 5786th episode, both the agent's reward value and the average reward value reach their highest points, 1871 and 1565, respectively, signaling the end of the training process. It can be observed that, after training, the controller is able to respond correctly and stably to random road inputs, optimizing the vehicle's dynamic parameters.

5.2. Simulation Result and Analysis

In MATLAB/Simulink, a random road profile with a road class C and vehicle speed of 40 km/h is used as the road spectrum input to simulate and verify the pump–valve joint EHA system with the DDPG control method. The parameters such as vertical acceleration, roll angle, and pitch angle of the vehicle are observed to validate the improvement in vehicle comfort, stability, and other driving performance with the DDPG-controlled EHA active suspension system. As a widely used method for solving nonlinear system control problems, the iLQR algorithm is based on simplified linear models and minimizes the error function through iterative optimization. This article compares the performance of the EHA active suspension controlled by DDPG with that controlled by iLQR and variable-damping semi-active suspension, demonstrating the superiority of the DDPG algorithm's performance. The agent training parameters and EHA system parameters are shown in Tables 2, 3.

TABLE 2 Training parameters.

Parameter	Value
Sample time	0.01
Simulation time	10
Max steps per episode	1000
Discount factor	0.99
Mini batch size	64
Experience buffer length	1,000,000
Standard deviation of action noise	0.5
Decay rate of standard deviation	0.001

As shown in Figures 7, 8, and Tables 4, 5, compared to the uncontrolled passive suspension, semi-active suspension improves ride comfort with variable-damping suspension adjustments. With random road inputs, the peak vertical acceleration of the vehicle decreased by 4.76%, and the RMS value decreased by 24.25%. The EHA active suspension controlled by iLQR demonstrated better performance. When processing random road input, the peak vertical acceleration of the vehicle decreased by 10.41%, and the RMS value decreased by 29.78%. Compared to the iLQR control method, the EHA active suspension controlled by DDPG showed the best performance. Under randomized road input conditions, the peak vertical acceleration of the vehicle decreased by 21.10%, and the RMS value decreased by 42.08%. Under convex packet road input conditions, the RMS value of vertical acceleration decreased by 44.54%.

Due to the higher ride comfort training weight used by the DDPG agent in this article, the optimization effect compared to the iLQR control method is more pronounced. However, it is also evident that the DDPG controller can optimize dynamic behavior, adapt to complex random road inputs, significantly reduce the magnitude of vertical acceleration, and provide a control performance clearly superior to the iLQR control method.

As shown in Figures 9–13, and Tables 6, 7, compared to the iLQR control method, the EHA active suspension controlled by DDPG also demonstrates a stronger ability to improve vehicle handling stability. Under iLQR control, the RMS value of the vehicle's pitch angle decreased by 20.06% compared to the uncontrolled passive suspension, and the RMS value of the vehicle's roll angle decreased by 11.62%. What's more, under randomized road input conditions, the RMS value of suspension dynamic deflection decreased by 6.45%. Under convex packet road input conditions, the RMS value of suspension dynamic deflection decreased by 23.21%.

FIGURE 6 Training results of DDPG controller.

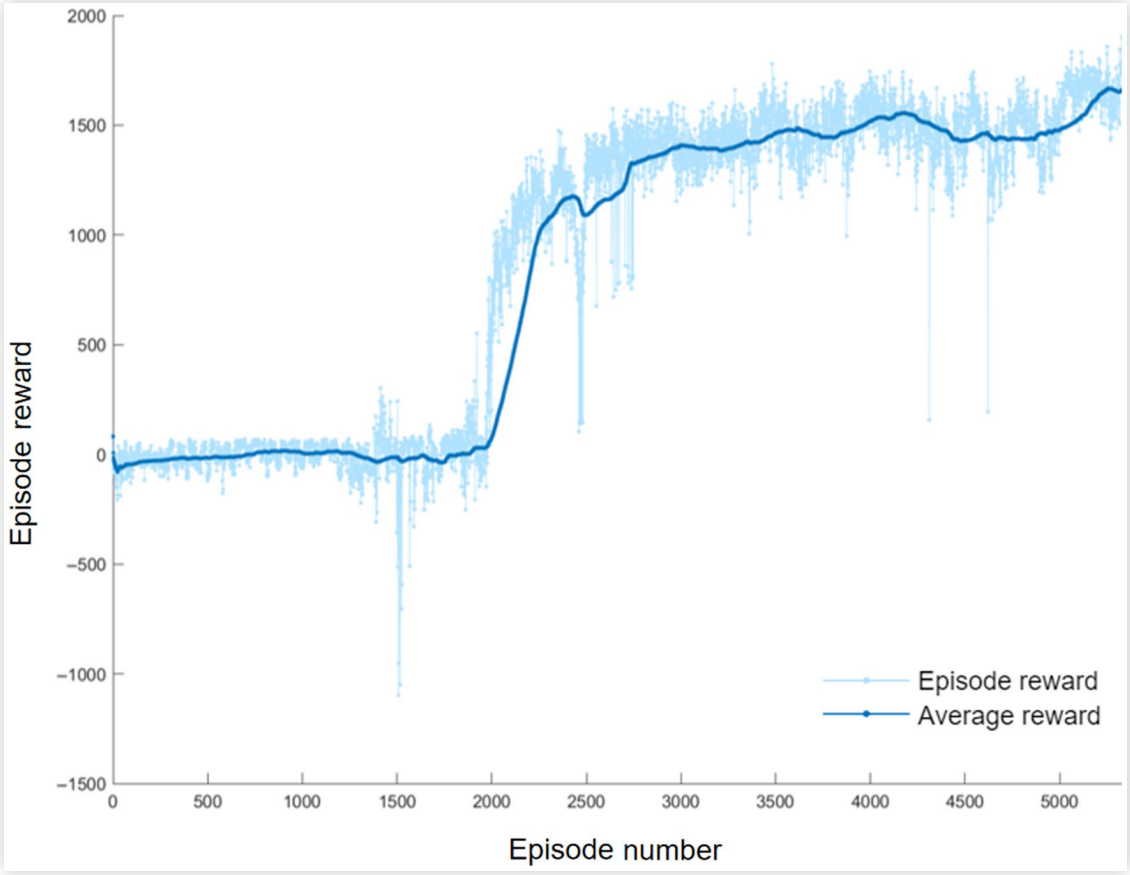

Under the DDPG control strategy, the RMS value of the vehicle's pitch angle decreased by 26.65% compared to the uncontrolled passive suspension, and the RMS value of the vehicle's roll angle decreased by 19.06%. Additionally, under randomized road input conditions, the RMS value of suspension dynamic deflection decreased by 12.90%. Under convex packet road inputs conditions, the RMS value of suspension dynamic deflection decreased by 34.17%. The DDPG controller responds more quickly to changes in the pitch angle, with smaller and smoother oscillations. In terms of roll angle control, the DDPG algorithm effectively suppresses the amplitude of roll angle variations, significantly improving lateral stability. The DDPG algorithm can learn attitude angle control strategies in complex environments, effectively improving the vehicle's stability and handling performance on uneven road surfaces.

As shown in Figure 14, the EHA active suspension under DDPG control can make optimal action decisions, and the displacement of the servo spool reciprocates between −0.005 m and 0.005 m, which effectively improves the servo valve's switching speed, and also improves the hydraulic cylinder's directional switching speed at the same time, so that it can deal with complex road inputs more comfortably. Under the iLQR control method, the servo spool displacement reaches a limit value of 0.01 m, which impacts the servo valve, and the servo valve's switching frequency is lowered, making it difficult to respond in time under complex road inputs. Therefore, DDPG's EHA active suspension control strategy effectively optimizes the efficiency and component life of the hydraulic components of the EHA system, and can more accurately control the actuator displacement and actuation force.

As shown in Figure 15, compared with the iLQR algorithm, the DDPG algorithm relies on its unique AC mechanism, which is more capable of controlling the nonlinear system. The valve front pressure controlled by the DDPG algorithm can respond quickly according to the random road inputs. Also, the valve front pressure is decreased significantly compared with the hydraulic system under iLQR control, which reduces the energy consumption of the system. Since the EHA pre-valve pressure under DDPG control responds at a rapid speed, as shown in the positioning control simulation curve in Figure 16, the EHA system takes less time to position itself to the reference position compared to the iLQR control.

FIGURE 7 Comparison of vehicle vertical acceleration control performance under random road inputs.

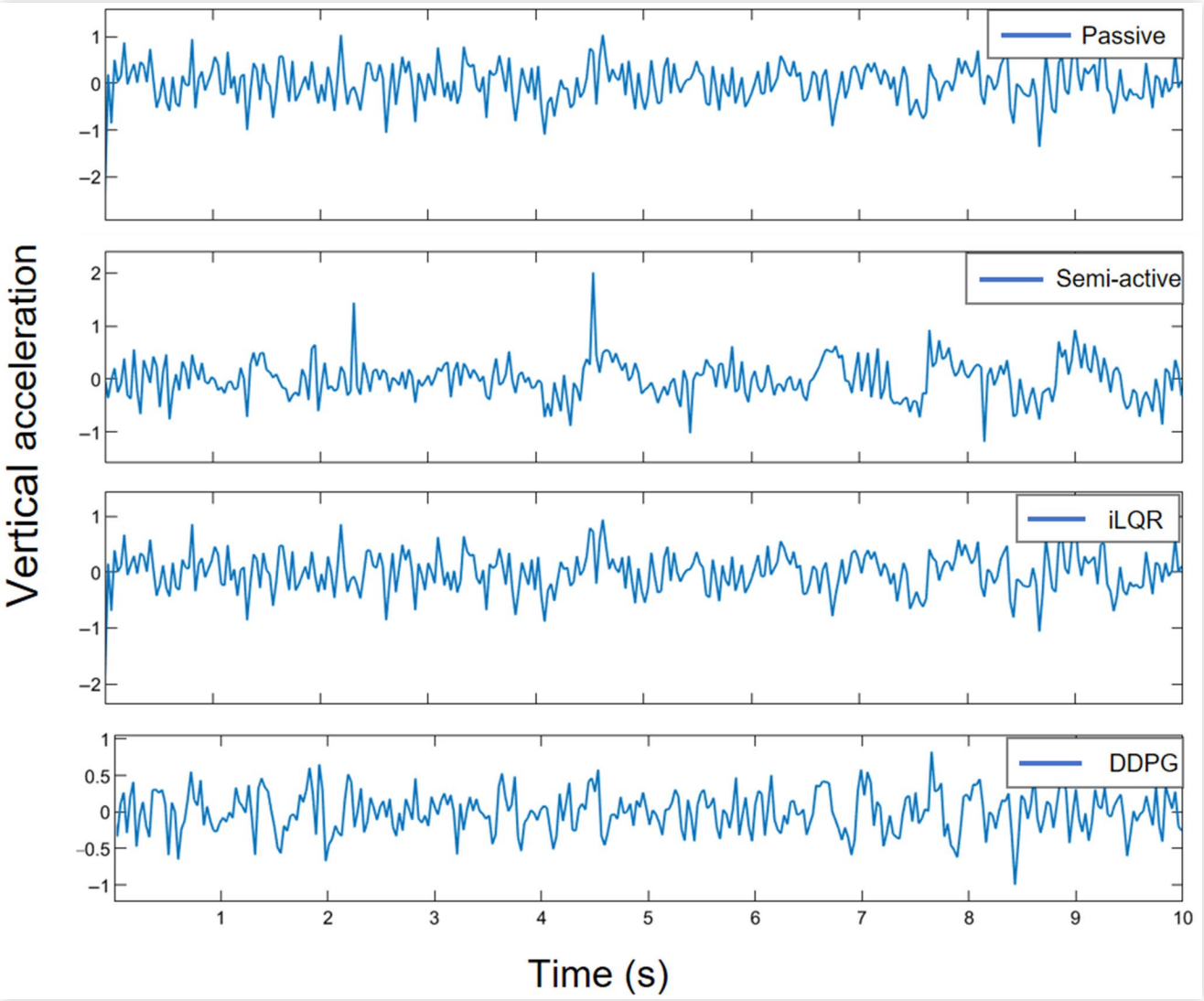

FIGURE 8 Comparison of vehicle vertical acceleration control performance under convex packet road inputs.

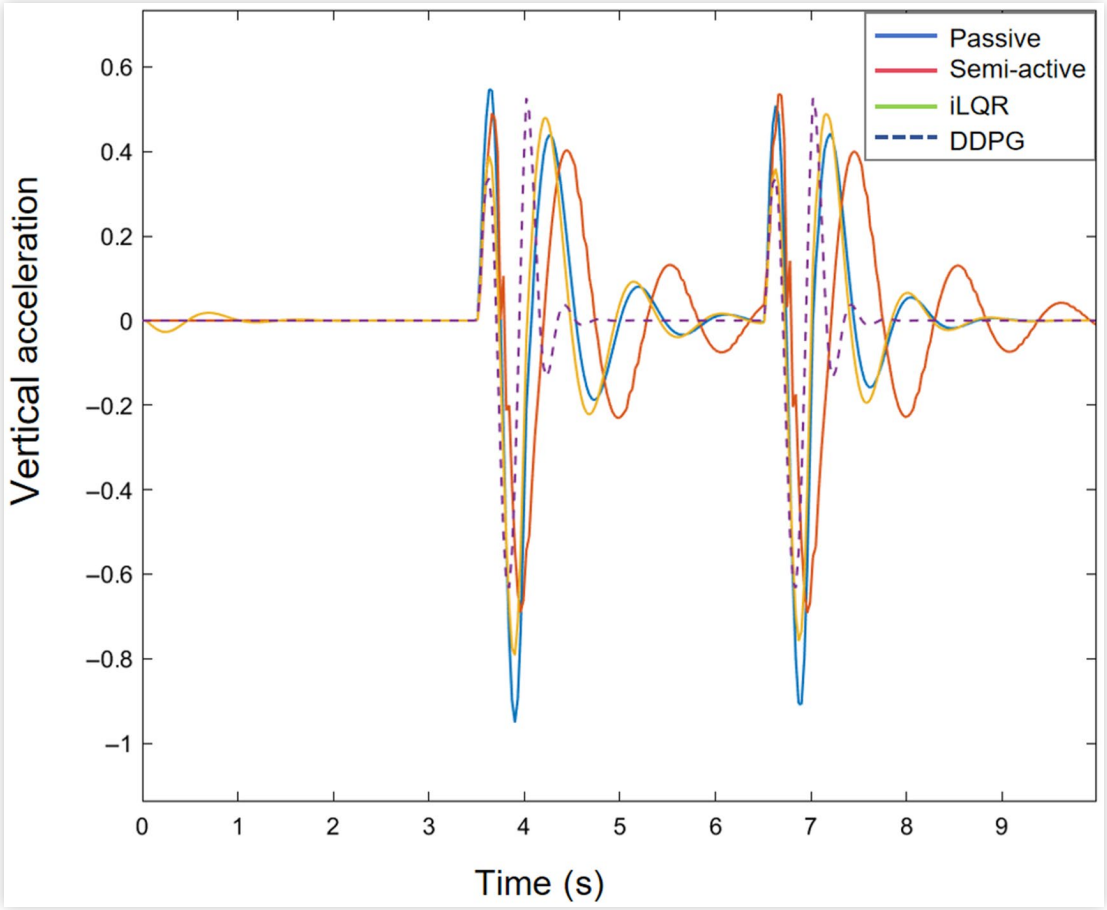

TABLE 4 Comparison of vehicle vertical acceleration peak value and RMS value under random road inputs.

Controller	Vertical acceleration peak value (m/s²)		Vertical acceleration RMS value (m/s²)	
	Value	Rate of change (%)	Value	Rate of change (%)
Passive suspension	3.526	—	0.9446	—
Semi-active suspension	3.358	−4.76	0.7155	−24.25
iLQR	3.159	−10.41	0.6633	−29.78
DDPG	2.782	−21.10	0.5471	−42.08

TABLE 5 Comparison of vehicle vertical acceleration peak value and RMS value under convex packet road inputs.

Controller	Vertical acceleration peak value (m/s²)		Vertical acceleration RMS value (m/s²)	
	Value	Rate of change (%)	Value	Rate of change (%)
Passive suspension	0.4789	—	0.2887	—
Semi-active suspension	0.4662	−2.65	0.2278	−21.01
iLQR	0.4467	−5.22	0.1879	−34.91
DDPG	0.4265	−34.92	0.1601	−44.54

FIGURE 9 Comparison of spring dynamic deflection control performance with random road inputs.

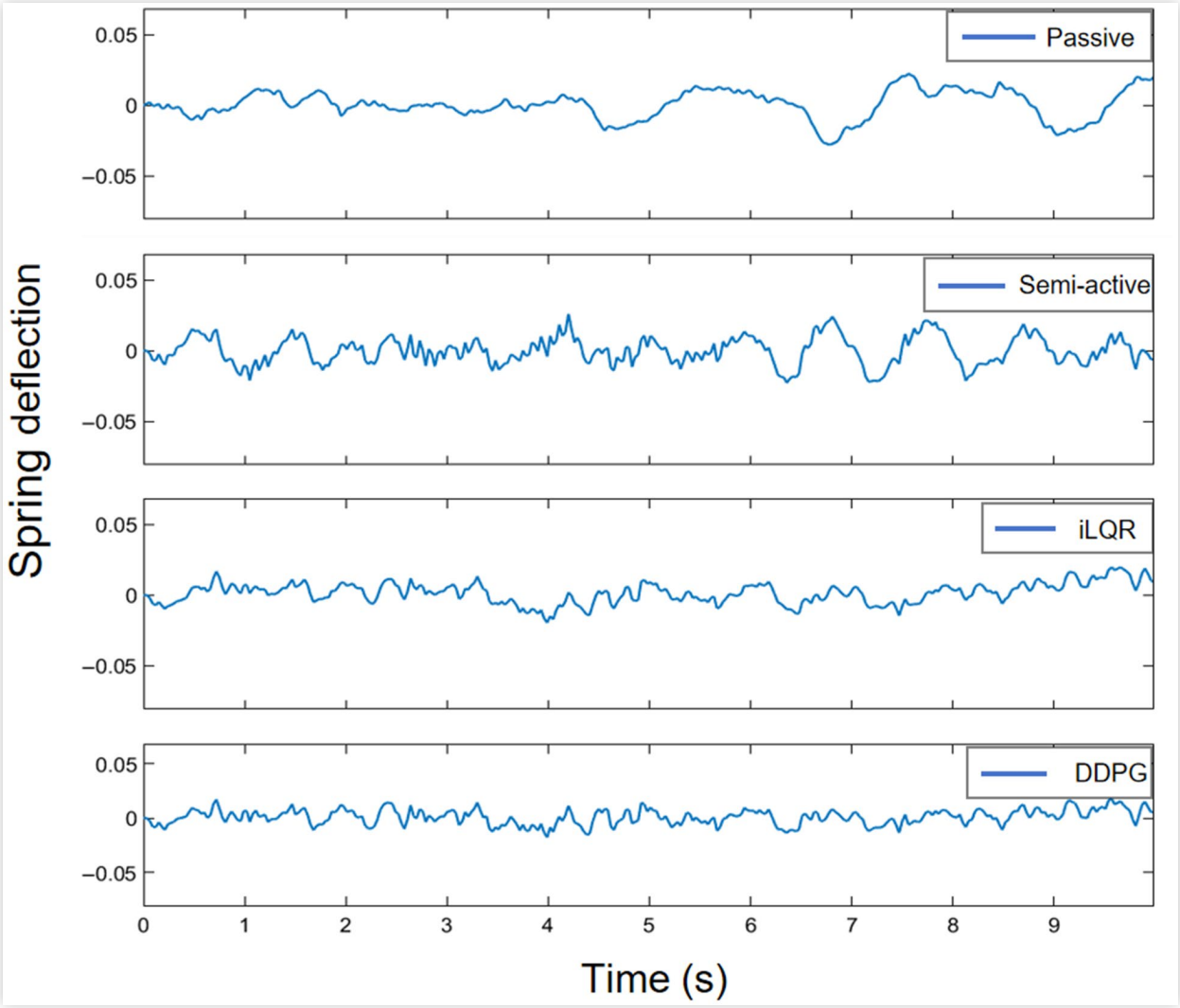

FIGURE 10 Comparison of spring dynamic deflection control performance with convex packet road inputs.

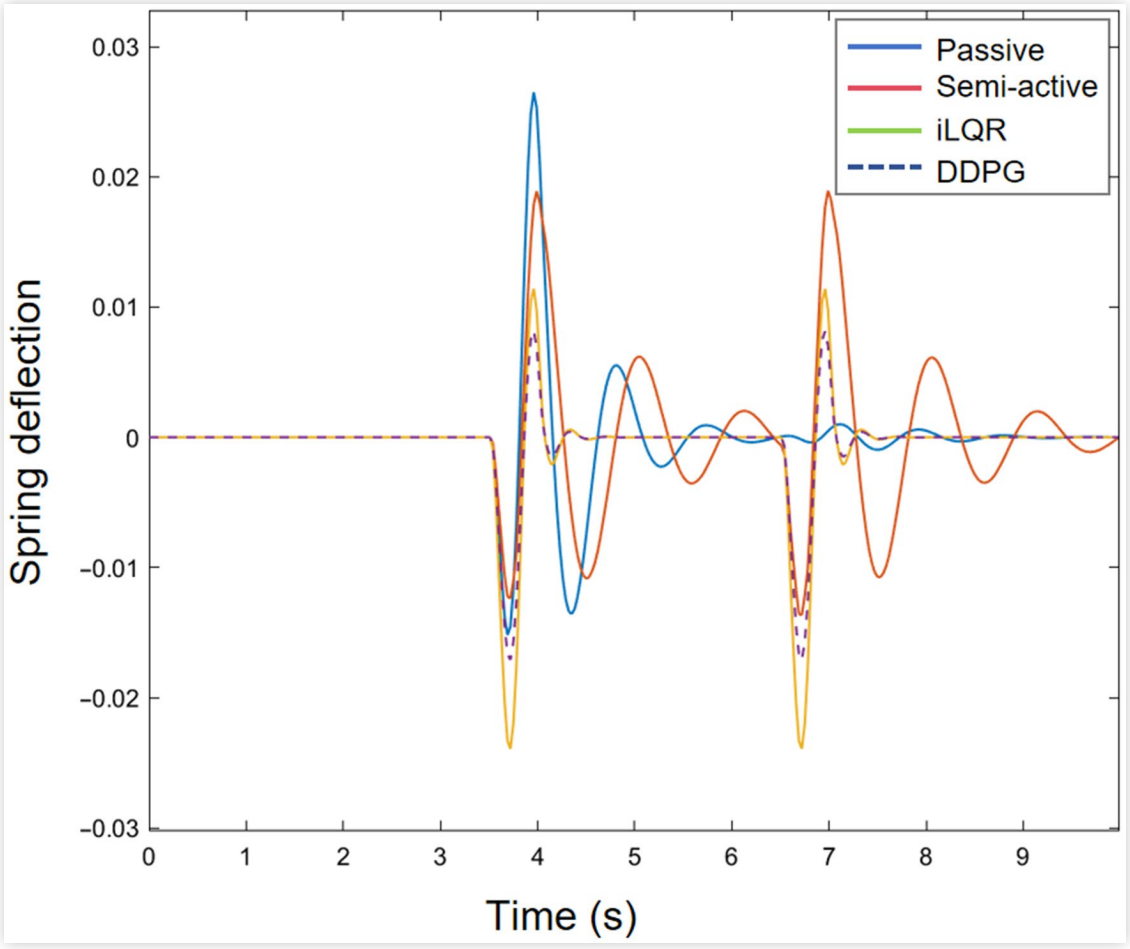

FIGURE 11 Comparison of the control effect of pitch angle with random road inputs.

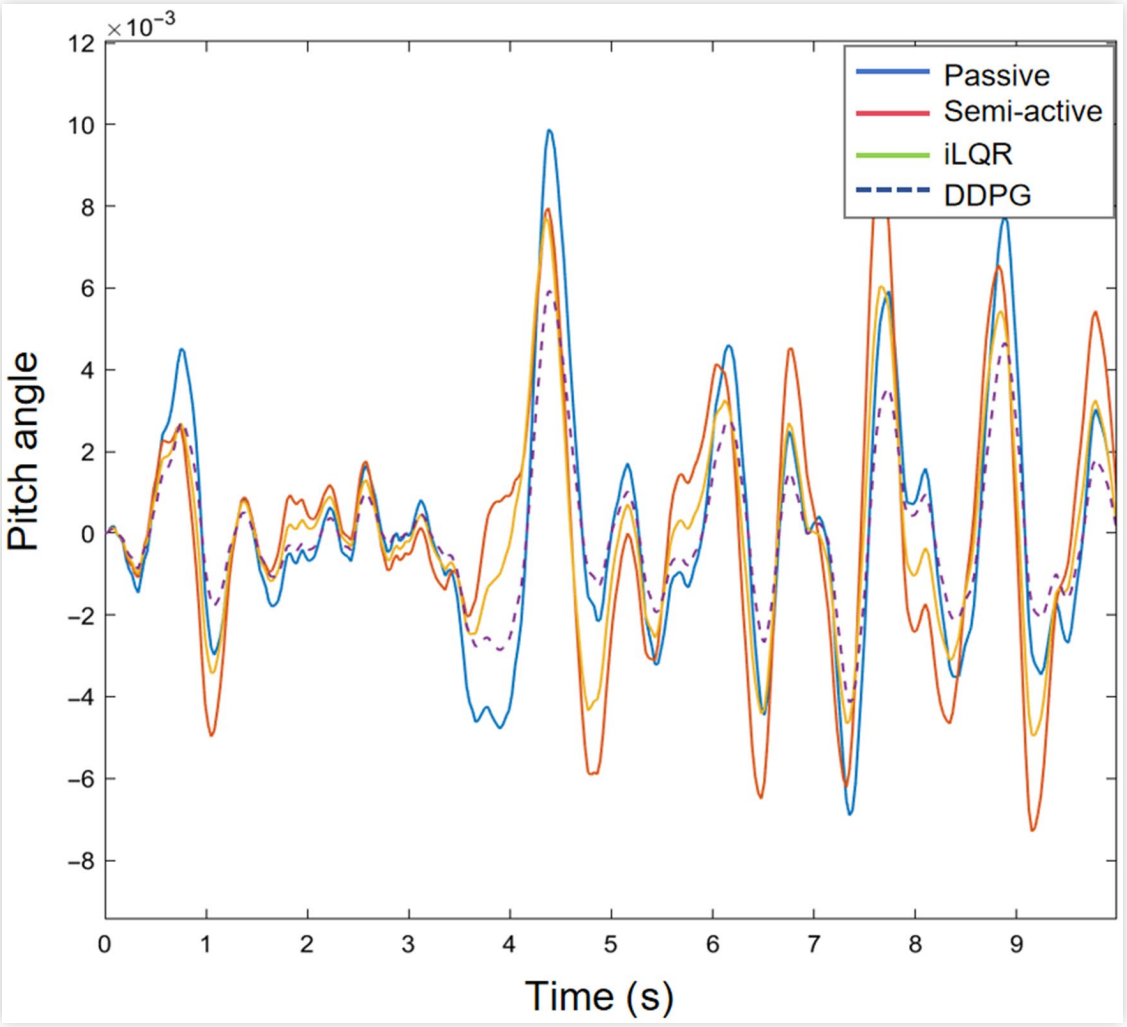

FIGURE 12 Comparison of the control effect of pitch angle with convex packet road inputs.

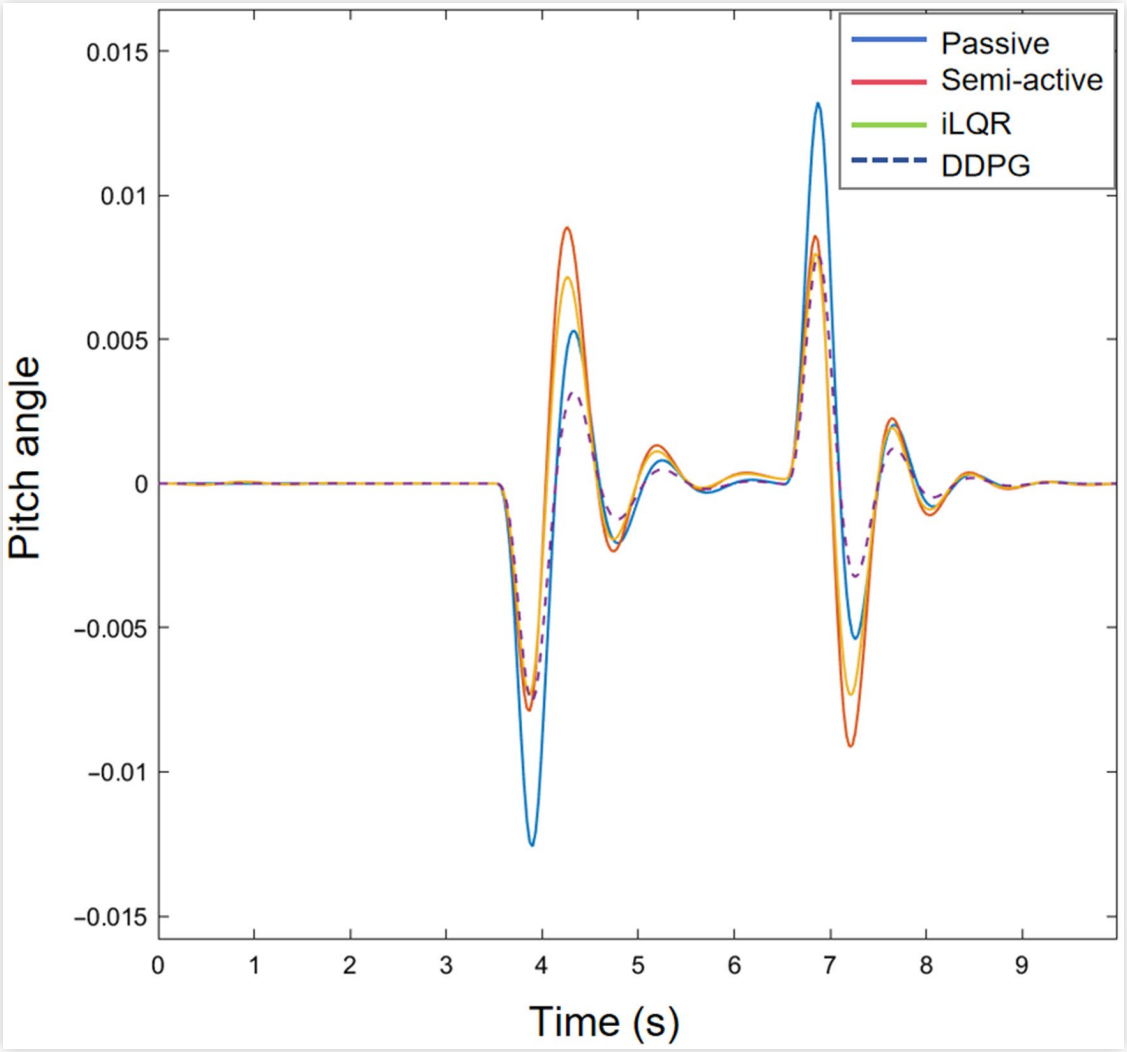

FIGURE 13 Comparison of the control effect of roll angle with random road inputs

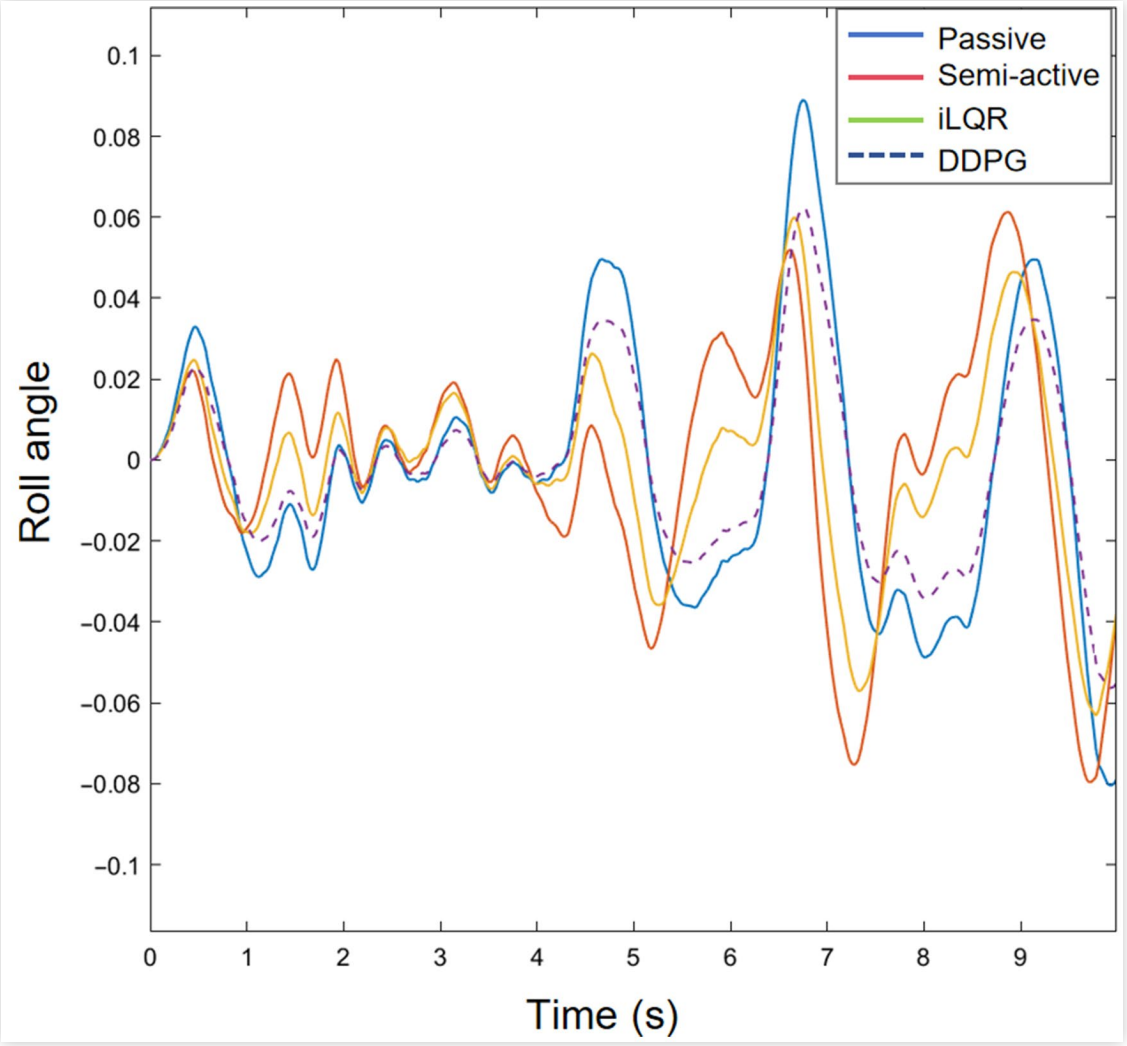

TABLE 6 Comparison of attitude angle and suspension dynamic deflection peak value and RMS value under random road inputs.

	peak value							RMS value						
Performance indicators	Passive suspension	Semi-active suspension	Rate of change (%)	iLQR	Rate of change (%)	DDPG	Rate of change (%)	Passive suspension	Semi-active suspension	Rate of change (%)	iLQR	Rate of change (%)	DDPG	Rate of change (%)
Spring dynamic deflection (m)	0.0278	0.0225	−19.06	0.0198	−28.78	0.0177	−36.33	0.00124	0.00118	−4.81	0.00116	−6.45	0.00108	−12.90
Pitch angle (rad)	0.0099	0.0092	−8.08	0.0077	−22.22	0.0069	−30.03	0.0030	0.0032	+6.67	0.0024	−20.06	0.0022	−26.65
Roll angle (rad)	0.0891	0.0797	−10.55	0.0632	−29.07	0.0623	−30.08	0.0327	0.0306	−6.42	0.0289	−11.62	0.0239	−19.06

TABLE 7 Comparison of attitude angle and suspension dynamic deflection peak value and RMS value under convex packet road inputs.

Performance indicators	Peak value							RMS value						
	Passive suspension	Semi-active suspension	Rate of change (%)	iLQR	Rate of change (%)	DDPG	Rate of change (%)	Passive suspension	Semi-active suspension	Rate of change (%)	iLQR	Rate of change (%)	DDPG	Rate of change (%)
Spring dynamic deflection (m)	0.0265	0.0237	−10.57	0.0211	−20.38	0.0202	−23.77	0.0043	0.0049	+13.95	0.0042	−2.33	0.0041	−4.76
Pitch angle (rad)	0.0132	0.0108	−13.60	0.0098	−25.76	0.0096	−27.27	0.0029	0.0026	+10.34	0.0022	−24.14	0.0020	−31.03
Roll angle (rad)	—	—	—	—	—	—	—	—	—	—	—	—	—	—

FIGURE 14 Comparison of servo valve displacement control.

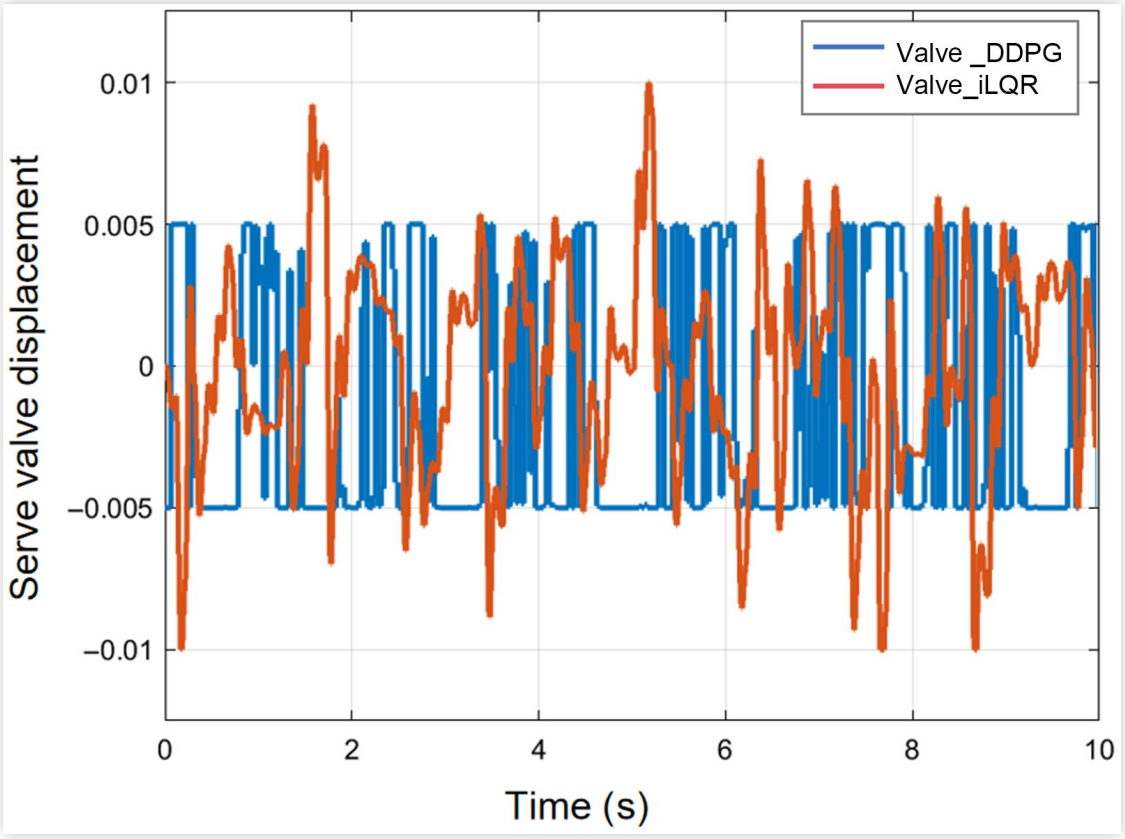

FIGURE 15 Comparison of EHA pre-valve pressure control effects.

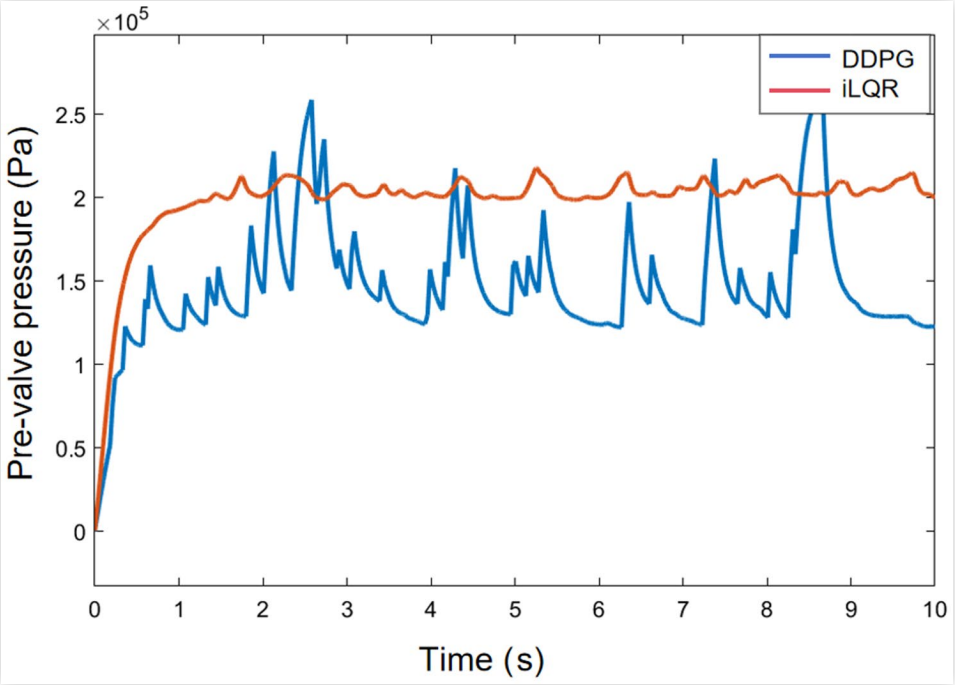

FIGURE 16 Comparison of reference displacement tracking.

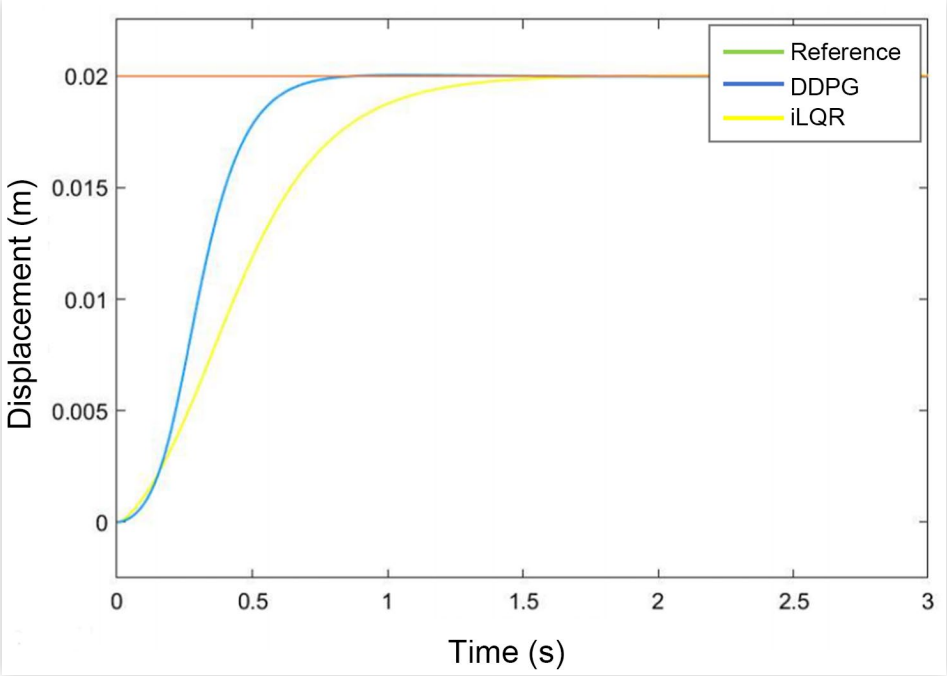

6. Conclusion and Future Work

6.1. Conclusion

1. First, to address the issues of high energy consumption, complex structure, and low reliability in active suspension systems, a hydraulic active suspension scheme based on EHA is proposed. Compared to pneumatic and electromagnetic active suspensions, EHA hydraulic active suspension features small volume, fast response, and high reliability, effectively reducing vehicle body vibrations and improving both comfort and handling.
2. Second, to address the nonlinear characteristics of hydraulic active suspension, this article proposes an EHA control strategy based on the DDPG deep learning algorithm. This strategy effectively reduces hydraulic shocks in the system while ensuring the actuator's response speed. After analyzing the 7-degrees-of-freedom vehicle dynamics model, the vertical acceleration and attitude angles of the vehicle's center of mass are observed. The vehicle dynamics parameters and EHA hydraulic system parameters are integrated into a reward function, and the optimization of the reward function is achieved during the training process of the DDPG agent.
3. In MATLAB/Simulink, a comparative simulation analysis is performed between the DDPG algorithm and the traditional iLQR algorithm to evaluate the control effects, verifying the improvement in vehicle ride comfort and handling stability when using the pump–valve joint EHA as an active suspension under the DDPG control strategy.

6.2. Future Work

Although the DDPG-based EHA active suspension control method shows significant advantages in addressing system nonlinearities and improving control accuracy, several directions still need further exploration:

1. First, although performance constraints on actuators are considered during DDPG training, it remains a black-box model with unclear decision logic and low interpretability. Future studies could integrate attention mechanisms and feature visualization to quantify neural network sensitivity to suspension states (e.g., body acceleration, suspension dynamic deflection), highlighting the physical meaning of the control strategy.
2. Second, the robustness and reliability of the DDPG control method under extreme operating conditions or system failures need further validation and optimization. Future research may combine robust control theory with DDPG to design a hybrid reinforcement learning framework, enhancing the safety and robustness of EHA active suspension systems in extreme conditions and complex road scenarios.

Advancing these research directions will promote the practical application of reinforcement learning algorithms in vehicle active suspension systems and accelerate the industrial deployment of intelligent active suspension technologies.

Acknowledgements

The work in this article was supported by the Independent Innovation Fund Project of Wuhan University of Technology. These financial supports are gratefully acknowledged by the authors.

Contact Information

Xiaohe Deng, corresponding author
333889@whut.edu.cn

Nomenclature

i_d - PMSM rotor straight-axis current
i_q - PMSM rotor cross -axis current
K_{fric} - Frictional resistance coefficient of vane pump
K_{visc} - Viscous resistance coefficient of vane pump
P_a - Inlet pressures of vane pump
P_b - Outlet pressures of vane pump
P_1 - Hydraulic cylinder high-pressure chamber pressure
P_2 - Hydraulic cylinder low-pressure chamber pressure
Q_b - Vane pump output flow rate
Q_L - Servo valve input port flow rate
T_e - PMSM electromagnetic torque
T_L - PMSM load torque
T_t - Vane pump driving torque
u_d - PMSM rotor straight-axis voltage
u_q - PMSM rotor cross-axis voltage
ρ - Fluid density

Abbreviations

AC - Actor-critic algorithm
DDPG - Deep deterministic policy gradient
DRL - Deep reinforcement learning
EHA - Electro-hydrostatic actuator
iLQR - Iterative linear quadratic regulator
PMSM - Permanent magnet synchronous motor
RL - Reinforcement learning
TD - Temporal difference

References

1. Tseng, H.E. and Hrovat, D., "State of the art Survey: Active and Semi-Active Suspension Control," *Vehicle System Dynamics* 53, no. 7 (2015): 1034-1062.
2. Yan, H.-F. and Yan, Y.-L., "Design of Automotive Active Suspension System and Simulation for Intelligent Control Strategy," *Journal of Computing* 35 (2024): 121-134.
3. Turcotte, J., East, W., and Plante, J., "Experimental Assessment of a Controlled Slippage Magnetorheological Automotive Active Suspension for Ride Comfort," *SAE Int. J. Veh. Dyn., Stab., and NVH* 6, no. 4 (2022): 357-370, doi:https://doi.org/10.4271/10-06-04-0024.
4. Shafiekhani, A. et al., "Design and Analysis of a Controller Using Quantitative Feedback Theory for a Vehicle Air Suspension System," *Systems and Control*, arXiv preprint arXiv:1710.10636, 2017, https://doi.org/10.48550/ARXIV.1710.10636.
5. Zhao, X.W. and Yang, H., "The Design and Analysis of New Hydraulic Energy-Regenerative Active Suspension Based on Adaptive Backstepping Sliding Mode Variable Structure Control," *Chinese Automation Congress (CAC)*, (2017): 4378-4382.
6. Luo, G. and Gorges, D., "Modeling and Adaptive Robust Force Control of a Pump-Controlled Electro-Hydraulic Actuator for an Active Suspension System," in *2019 IEEE Conference on Control Technology and Applications (CCTA)*, Hong Kong, China, 2019, 592-597, https://doi.org/10.1109/ccta.2019.8920451.
7. Kou, F.R., "Sky-Hook Control of Vehicle Active Suspension with Electro-Hydrostatic Actuator," *Advanced Materials Research* 846–847 (2013): 30-33.
8. Kou, F., Wang, Z., Du, J., Li, D. et al., "Study on Force Tracking Control of Electro-Hydraulic Active Suspension," in *2017 IEEE 3rd Information Technology and Mechatronics Engineering Conference (ITOEC)*, Chongqing, China, 2017, 1078-1082, https://doi.org/10.1109/itoec.2017.8122520.
9. Miki, T., Lee, J., Hwangbo, J., Wellhausen, L. et al., "Learning Robust Perceptive Locomotion for Quadrupedal Robots in the Wild," *Science Robotics* 7, no. 62 (2022): eabk2822.
10. Roy, N. et al., "From Machine Learning to Robotics: Challenges and Opportunities for Embodied Intelligence," *Robotics*, arXiv preprint arXiv:2110.15245, 2021.
11. Abadi, M. et al., "TensorFlow: Large-Scale Machine Learning on Heterogeneous Distributed Systems," *Distributed, Parallel, and Cluster Computing*, arXiv preprint arXiv:1603.04467, 2016.
12. Hippalgaonkar, K. et al., "Knowledge-Integrated Machine Learning for Materials: Lessons from Gameplaying and Robotics," *Nature Reviews Materials* 8 (2023): 241-260.
13. Ma, R. et al., "Position and Attitude Tracking Control of a Biomimetic Underwater Vehicle via Deep Reinforcement Learning," *IEEE/ASME Transactions on Mechatronics* 28 (2023): 2810-2819.
14. Chen, Y. et al., "Deep Reinforcement Learning in Autonomous Car Path Planning and Control: A Survey," *Robotics*, arXiv preprint arXiv:2404.00340, 2024.
15. Gheni, E.Z., Al-Khafaji, H.M., and Alwan, H.M., "A Deep Reinforcement Learning Framework to Modify LQR for an Active Vibration Control Applied to 2D Building Models," *Open Engineering* 14, no. 1 (2024): 20220496, doi:https://doi.org/10.1515/eng-2022-0496.
16. Lillicrap, T.P., Hunt, J.J., Pritzel, A., Heess, N. et al., "Continuous Control with Deep Reinforcement Learning," *Machine Learning*, arXiv preprint arXiv:1509.02971, 2015.

Appendix

7-DOF Vehicle Dynamics Equations

According to Newton's second law, the vehicle's 7-degree-of-freedom dynamics equations are established. First, the parameters appearing in the 7-degrees-of-freedom model are defined as follows: m_b is the mass of vehicle body; I_p is the body pitch rotational inertia; I_r is the body roll rotational inertia; a_f is the distance from the front axle to the body's center of mass; b_r is the distance from the rear axle to the body's center of mass; $\ddot{z}_b$ is the vertical acceleration of vehicle body; $K_{sA\sim D}$ are relatively the spring stiffness of each suspension; $C_{sA\sim D}$ are relatively the damping of each suspension; $z_{wA\sim D}$ are relatively the vertical displacements of each wheel; $\dot{z}_{wA\sim D}$ are relatively the four end point displacement velocities of each wheel; $z_{bA\sim D}$ are relatively the four end point displacements of the body; $\dot{z}_{bA\sim D}$ are relatively the four end point displacement velocities of each wheel; F_{alf} is the left front active suspension actuator force; F_{arf} is the right front active suspension actuator force; F_{alr} is the left rear active suspension actuator force; F_{arr} is the right rear active suspension actuator force.

Body Motions

Vertical:

$$\begin{aligned} m_b\ddot{z}_b = {} & C_{sA}\left(\dot{z}_{wA}-\dot{z}_{bA}\right)+K_{sA}\left(z_{wA}-z_{bA}\right)+C_{sB}\left(\dot{z}_{wB}-\dot{z}_{bB}\right) \\ & +K_{sB}\left(z_{wB}-z_{bB}\right)+C_{sC}\left(\dot{z}_{wC}-\dot{z}_{bC}\right)+K_{sC}\left(z_{wC}-z_{bC}\right) \\ & +C_{sD}\left(\dot{z}_{wD}-\dot{z}_{bD}\right)+K_{sD}\left(z_{wD}-z_{bD}\right)-\left(F_{alf}+F_{alr}+F_{arf}+F_{arr}\right) \end{aligned} \tag{A.1}$$

Pitch:

$$\begin{aligned} I_p\ddot{\theta} = {} & \left(C_{sC}\left(\dot{z}_{wC}-\dot{z}_{bC}\right)+K_{sC}\left(z_{wC}-z_{bC}\right)+C_{sD}\left(\dot{z}_{wD}-\dot{z}_{bD}\right)\right. \\ & +K_{sD}\left(z_{wD}-z_{bD}\right)-\left(F_{alr}+F_{arr}\right))*b-a^*(C_{sA}\left(\dot{z}_{wA}-\dot{z}_{bA}\right) \\ & \left.+K_{sA}\left(z_{wA}-z_{bA}\right)+C_{sB}\left(\dot{z}_{wB}-\dot{z}_{bB}\right)+K_{sB}\left(z_{wB}-z_{bB}\right)-\left(F_{alf}+F_{arf}\right)\right) \end{aligned} \tag{A.2}$$

Roll:

$$\begin{aligned} I_r\ddot{\phi} = {} & \left(-C_{sA}\left(\dot{z}_{wA}-\dot{z}_{bA}\right)-K_{sA}\left(z_{wA}-z_{bA}\right)+C_{sB}\left(\dot{z}_{wB}-\dot{z}_{bB}\right)\right. \\ & +K_{sB}\left(z_{wB}-z_{bB}\right)-\left(F_{arf}-F_{alf}\right))*\frac{B_f}{2}-\frac{B_r}{2}*(C_{sC}\left(\dot{z}_{wC}-\dot{z}_{bC}\right) \\ & \left.+K_{sC}\left(z_{wC}-z_{bC}\right)+C_{sD}\left(\dot{z}_{wD}-\dot{z}_{bD}\right)+K_{sD}\left(z_{wD}-z_{bD}\right)-\left(F_{arr}-F_{alr}\right)\right) \end{aligned} \tag{A.3}$$

The four end point displacements of the body are as follows:

$$\begin{aligned} z_{bA} &= z_b-a\theta-\frac{1}{2}B_f\phi \\ z_{bB} &= z_b-a\theta+\frac{1}{2}B_f\phi \\ z_{bC} &= z_b+a\theta-\frac{1}{2}B_f\phi \\ z_{bD} &= z_b+a\theta+\frac{1}{2}B_f\phi \end{aligned} \tag{A.4}$$

Wheel Dynamics

The vertical equations of the wheels' motion at each suspension are:

$$\begin{aligned} m_{wA}\ddot{z}_{wA} &= K_{tA}\left(z_{gA}-z_{wA}\right)+K_{sA}\left(z_{bA}-z_{wA}\right)+C_{sA}\left(\dot{z}_{bA}-\dot{z}_{wA}\right)+F_{alf} \\ m_{wB}\ddot{z}_{wB} &= K_{tB}\left(z_{gB}-z_{wB}\right)+K_{sB}\left(z_{bB}-z_{wB}\right)+C_{sB}\left(\dot{z}_{bB}-\dot{z}_{wB}\right)+F_{arf} \\ m_{wC}\ddot{z}_{wC} &= K_{tC}\left(z_{gC}-z_{wC}\right)+K_{sC}\left(z_{bC}-z_{wC}\right)+C_{sC}\left(\dot{z}_{bC}-\dot{z}_{wC}\right)+F_{alr} \\ m_{wD}\ddot{z}_{wD} &= K_{tD}\left(z_{gD}-z_{wD}\right)+K_{sD}\left(z_{bD}-z_{wD}\right)+C_{sD}\left(\dot{z}_{bD}-\dot{z}_{wD}\right)+F_{arr} \end{aligned} \tag{A.5}$$